Activation of the astrocytic Nrf2/ARE system ameliorates the formation of demyelinating lesions in a multiple sclerosis animal model

Draheim T.[1]*, Liessem A.[1]*, Scheld M.[1], Wilms F.[1], Weißflog M.[1], Denecke B.[2], Kensler TW.[4], Zendedel A.[1;5], Beyer C.[1], Kipp M.[1;6], Wruck CJ.[3] Fragoulis A.[3;7#], Clarner T[1].#

1) Institute of Neuroanatomy, Faculty of Medicine, Uniklinik RWTH Aachen, 52074 Aachen, Germany

2) Interdisciplinary Centre for Clinical Research (IZKF) Aachen, Uniklinik RWTH Aachen, 52074 Aachen, Germany

3) Department of Anatomy and Cell Biology, Faculty of Medicine, Uniklinik RWTH Aachen, 52074 Aachen, Germany

4) Department of Pharmacology and Chemical Biology, School of Medicine, University of Pittsburgh, Pittsburgh, PA 15261, U.S.A.

5) Department of Anatomical Sciences, Faculty of Medicine, Giulan University of Medical Sciences, Rasht, Iran

6) Department of Anatomy II, Ludwig-Maximilians-University of Munich, Munich, Germany

7) Department of Orthopaedic Surgery, Faculty of Medicine, Uniklinik RWTH Aachen, 52074 Aachen

Running title: Astrocytic Nrf2 hyperactivation prevents the formation of demyelinating lesions

Word counts:

Abstract: 171
Introduction: 956
Materials and methods: 1634
Results: 1285
Discussion: 1064
Total words: 5110

Main points:
The activation of the astrocytic Nrf2/Are system ameliorates oligodendrocyte loss, microglia activation and demyelination in an animal model of multiple sclerosis.

Corresponding author:
Tim Clarner, Dr. rer. nat.
Institute of Neuroanatomy, Medical Faculty, RWTH Aachen University, Wendlingweg 2, 52074 Aachen, Germany, phone: 00 49 (0)241 8037669, Email: tclarner@ukaachen.de

*
  both authors contributed equally as first authors

# both authors contributed equally as last authors

Abstract:

Oxidative stress critically contributes to the pathogenesis of a variety of neurodegenerative diseases such as multiple sclerosis. Astrocytes are the main regulators of oxidative homeostasis in the brain and dysregulation of these cells likely contributes to the accumulation of oxidative damage. The nuclear factor erythroid 2-related factor 2 (Nrf2) is the main transcriptional regulator of the anti-oxidant stress defense. In this study, we elucidate the effects of astrocytic Nrf2-activation on brain-intrinsic inflammation and lesion development. Cells deficient for the Nrf2 repressor kelch-like ECH-associated protein 1 (Keap1) are characterized by hyperactivation of Nrf2-signaling. Therefore, wild type mice and mice with a GFAP-specific Keap1-deletion were fed with 0.25% cuprizone for 1 or 3 weeks. Cuprizone intoxication induced pronounced oligodendrocyte loss, demyelination and reactive gliosis in wild type animals. In contrast, astrocyte-specific Nrf2-activation was sufficient to prevent oligodendrocyte loss and demyelination, to ameliorate brain intrinsic inflammation and to counteract axonal damage. Our results highlight the potential of the Nrf2/ARE system for the treatment of neuroinflammation in general and of multiple sclerosis in particular.

Introduction

Multiple sclerosis (MS) is an inflammatory disorder of the central nervous system (CNS) with a heterogeneous disease course and complex pathophysiology. Different conflicting concepts have been proposed to explain disease progression and lesion formation in MS (Mahad et al. 2015). Although the inflammatory responses greatly differ among distinct MS lesion subtypes, overall data suggests that considerable brain-intrinsic inflammation and an activation of microglia cells are always present when active demyelination or neurodegeneration occurs (Frischer et al. 2009; Mahad et al. 2015). Reactive microglia are thought to contribute to tissue damage by the secretion of inflammatory mediators such as cytokines and chemokines, as well as the production of reactive oxygen (ROS) and nitrogen species (RNS). Indeed, signs of oxidative damage such as oxidized phospholipids and malondialdehyde (MDH) in myelin, apoptotic oligodendrocytes, degenerating glia cells and neurons indicate a critical role of oxidative stress for the pathogenesis of MS lesions (Haider et al. 2011; Lu et al. 2000; van Horssen et al. 2008). Persistent oxidative stress likely exacerbates the already deleterious effects of the neuroinflammation itself (Johnson and Johnson 2015; Lassmann 2014; Schuh et al. 2014).

The role of activated astrocytes within damaged brain areas is complex and manifold. Astroglial (dys)-function can result in demyelination and oligodendrocyte pathology (Sharma et al. 2010). It is furthermore documented that activated astrocytes secrete molecules with potentially direct toxic effects on neurons/axons and oligodendrocytes/myelin, such as ROS and RNS, glutamate, and ATP (Spray 2011). For example, extensive iNOS reactivity was observed in hypertrophic astrocytes in acute MS lesions (Liu et al. 2001). Despite this detrimental role, beneficial effects of astrocytes on de- and remyelination are also discussed. The detoxification of free radicals in the CNS has been linked to astrocytes in a variety of diseases such as spinal cord ischemia, amyotrophic lateral sclerosis as well as Parkinson`s and Alexander`s disease (Mena and Garcia de Yebenes 2008).

The nuclear factor erythroid 2-related factor 2 (Nrf2) is a key molecule involved in the transcriptional regulation of multiple oxidative-stress-related genes in the insulted brain (Dang et al. 2012). Among activation by oxidative challenge, Nrf2 is released from its repressor kelch-like ECH-associated protein 1 (Keap1) and translocates into the nucleus where it binds to the antioxidant response element (ARE), thereby activating the transcription of antioxidant and detoxifying enzymes (Huang et al. 2015). Pharmacological activation of the Nrf2/ARE system has proven beneficial in a variety of diseases, among MS (Al-Sawaf et al. 2015; Wruck et al. 2008). Recently, the dimethyl fumaric acid ester compound dimethyl fumarate (DMF, also known as BG-12, Fumaderm) was approved for the treatment of relapsing-remitting MS (Kim et al. 2015). Although the mechanism of action is not completely understood, it has been shown that DMF activates Nrf2-activity by disruption of the Nrf2 - Keap1 interaction due to a modification at cysteine residue 151 of

the Keap1 protein (Linker et al. 2011). This leads to increased Nrf2-signaling, both *in vivo* and *in vitro*. However, other mechanisms seem more likely to contribute to DMF efficacy, such as an activation of Hydroxycarboxylic acid receptor 2 (Chen et al. 2014; Offermanns and Schwaninger 2015). Besides, it has recently been shown that DMF sufficiently inhibits NF-κB in an Nrf2-independend manner (Gillard et al. 2015). Further studies are therefore needed to clarify the precise effects of activation of Nrf2-signaling in distinct cell types and pathologies. As already mentioned for DMF, all known Nrf2-inducers not only enhance Nrf2-activity but also exert various additional effects within the brain and peripheral tissues (Fragoulis et al. 2012). Therefore, genetic and cell type specific targeting of Keap1 and/or Nrf2 represents the most suitable method to investigate Nrf2-specific effects.

With respect to MS, experimental autoimmune encephalomyelitis (EAE) is exacerbated in Nrf2-KO mice, demonstrating the relevance of Nrf2 for autoimmune neuroinflammatory responses (Johnson et al. 2010). In contrast to EAE, T cells are not the driving pathogenic force in the cuprizone model of MS (Kipp et al. 2009). This model allows studying the basic mechanisms of de- and remyelination, since no interference by the peripheral immune system takes place. It is characterized by reproducible demyelination within both white and gray matter, a selective and pronounced loss of oligodendrocytes and robust micro- and astrogliosis within damaged brain regions (Clarner et al. 2015; Goldberg et al. 2015; Slowik et al. 2015). Using this model of demyelination, we investigated the effects of astrocyte-specific, persistent hyperactivation of Nrf2 signaling on reactive gliosis and subsequent oxidative damage.

Materials and Methods

Animals

Animals were fed a diet containing 0.25% cuprizone (bis-cyclohexanone oxaldihydrazone; Sigma-Aldrich) in powdered standard rodent chow for the indicated period. Control mice were provided with standard rodent chow as published previously (Clarner et al. 2015). Animals had free access to food and water and were housed under standard laboratory and pathogen free conditions according to the Federation of European Laboratory Animal Science Association's recommendations. The procedures were approved by the Review Board for the Care of Animal Subjects of the district government (North-Rhine Westphalia, Germany) and performed according to international guidelines on the use of laboratory mice.

Early (1 week cuprizone) and late (3 weeks cuprizone) demyelinating lesions were induced in different mouse strains on the C57BL/6J background with appropriate littermates as controls (see below). If not stated otherwise, the current study was conducted with 8 to 16 week old mice. The following mouse strains were included:

- C57BL/6J ARE luciferase reporter gene mice (Cgene, Oslo) (Dohlen et al. 2008) to visualize

Nrf2-activation in early lesions (1 week). Untreated C57BL/6J ARE luciferase reporter gene mice were included as controls.

- *GFAP-Cre::keap1$^{flox/flox}$* KO (referred to as Keap1-KO in this manuscript) mice were generated by cross-breeding homozygous floxed Keap1$^{flox/flox}$ with mice expressing Cre recombinase under the control of the glial fibrillary acidic protein (GFAP) promoter. The GFAP-Cre expressing mouse was kindly provided by Prof. Lüdde (Faculty of medicine, Uniklinik RWTH Aachen, Germany). The astrocyte-specific expression of the Cre recombinase in this strain was described in (Bajenaru et al. 2002). Keap1$^{flox/flox}$ animals were already available as Alb-Cre::Keap1$^{flox/flox}$ strain in our group and were initially provided by Prof. Kensler (Department of Pharmacology and Chemical Biology, School of Medicine, University of Pittsburgh, Pittsburgh, PA USA). For cross-breeding, Cre-negative Keap1$^{flox/flox}$ animals were mated with GFAP-Cre expressing mice. As in this strain's Cre recombinase is specifically expressed by astrocytes, these animals lack astrocytic Keap1. This leads to a hyperactivation of the Nrf2/ARE system in the targeted cells as also demonstrated for hepatocytes by Okawa and colleagues using an Albumin-driven Cre recombinase (Okawa et al. 2006). There was no histological phenotype found due to the Keap1 ablation. Cre negative animals with floxed Keap1 alleles served as controls in this approach. These mice were used to investigate the protective effects of astrocyte-specific Nrf2/ARE-activation in the brains of mice fed cuprizone for 3 weeks.

In vivo visualization of ARE-activity

Age and weight-matched littermates (8-16 weeks of age and 19-25g of body weight) were used for ARE-activity measurements (n = 5/group). Heads were shaved to allow a more sufficient luminescence imaging through skin and skull. Luciferin injection solution (Synchem OHG, Felsberg/ Altenburg, Germany) was prepared under sterile conditions as published previously (Fet et al. 2014) and used at a final concentration of 20 mg/mL. 0.2mL luciferin solution was injected intraperitoneally 10 min before narcotization. Mice were anesthetized by inhaling 5% (v/v) isoflurane (AbbVie, Ludwigshafen, Germany) at a flow rate of 2 L/min oxygen for approximately 1 min and then kept at 1.5% (v/v) and 1 L/min using a mouse face mask. Body temperature was maintained at 37.0 ± 0.5 °C with an electrical heating pad.

Fifteen minutes after luciferin injection, mice were imaged for 5 min from the dorsal side at high-resolution settings (binning: 2, f/stop: 1) with a field of view of 7.5 cm. Emitted light was detected by the IVIS Imaging System 100 Series (Xenogen Corporation, Alameda, CA), digitized and evaluated using the Living Image software 3.2 (Xenogen Corporation, Alameda, CA). Brain-specific signals were quantified using defined regions of interest (ROIs). Obtained luminescence signals were

normalized to the signals of control mice from the very same measurement. Results are thereby expressed as relative luminescence values (n-fold). The false color scale of the corresponding measurement and pictures is presented as photons/sec/cm²/sr. Non-specific background signals were subtracted as published previously (Wruck et al. 2011).

To investigate region specific luciferase-activity in the brain, mice were injected as described above and killed 10 min later by cervical dislocation. Brains were quickly removed, sliced into 1 mm thick coronal sections and imaged as described above.

Tissue preparation

For histological and immunohistochemical (IHC) studies, mice were transcardially perfused with 3.7% paraformaldehyde in 10 mM PBS. After overnight post-fixation in the same fixative, brains were dissected, embedded in paraffin, and then coronary sectioned into 5 μm sections at the levels 235 and 265 according to the mouse brain atlas of Sidman et al. (http://www.hms.harvard.edu/research/brain/atlas.html).

For gene expression analysis and lipid peroxidation assays, mice were deeply anesthetized and transcardially perfused with ice-cold PBS, the brains quickly removed, and the entire corpus callosum dissected using a stereomicroscopic approach. Isolated tissue was snap-frozen in liquid nitrogen and kept at −80 °C until further used (Clarner et al. 2015).

Gene expression studies

For this study, a previously published Gene array was re-evaluated focusing on oxidative-stress pathways and Nrf2-activation (Krauspe et al. 2015). For real time PCR (RT-qPCR) studies, tissue was homogenized in PeqGold RNA Pure (PeqLab, Germany; cat. no. 30-1010) and RNA isolated according to the manufacturer's protocols. RNA concentration and purity were photometrically measured on a NanoDrop 1000 (Thermo Fisher Scientific, USA). Reverse transcription was performed using 1 μg of total RNA and a MMLV reverse transcriptase kit (Invitrogen, Germany, 28025-013) (Clarner et al. 2014). qRT-PCR utilizing SYBR Green SensiMixTM (Bioline, Germany, QT615-05) was carried out on the MyIQ RT-PCR detection system (Biorad, Germany) applying the following protocol: 10 min enzyme activation at 95°C, 40 cycles of 15 s denaturation at 95°C, 30 s annealing at individual temperatures, 30 s amplification at 72 °C, and 5 s fluorescence measurement at 80°C. Relative quantification of gene expression was performed with the efficacy-corrected ΔCt method and data normalized to a reference gene. Primer sequences and annealing temperatures are given in Table 2 (Clarner et al. 2014). For amplification-efficacy determination, external standard curves were generated by several fold dilutions of cDNA samples used in the respective experiment. The target gene expression was calculated by comparing relative expression in each sample with respective

reference gene values. Finally, data was normalized and related to the expression of control groups. Melting curves and gel electrophoresis of the PCR products were routinely performed to determine the specificity of the PCR reaction (not shown) (Groebe et al. 2009).

Immunohistochemistry (IHC) and luxol fast blue staining

For IHC, sections were placed on glas slides, deparaffinized, rehydrated, heat unmasked if necessary, blocked with PBS containing 5% horse or normal goat serum, and incubated overnight at 4 C with the primary antibody diluted in blocking solution. Primary antibodies and dilutions used in the study are given in Table 3. After washing and blocking of endogenous peroxidase with 0.3% hydrogen peroxide (in PBS) for 30 min, sections were incubated with biotinylated secondary horse anti-mouse or goat anti-rabbit antibody diluted in blocking solution for 1 h, followed by peroxidase-coupled avidin–biotin complex (ABC kit; Vector Laboratories). The diaminobenzidine reaction (DAKO Deutschland) was used to visualize peroxidase–avidin–biotin complexes. Sections were counterstained with standard hematoxylin to visualize cell nuclei. Secondary antibodies and dilutions used are given in Table 4.

To assess cell-specific expression of Nrf2, immunofluorescence double stainings were performed. Therefore, slides were blocked with 2% FCS, 0.05% Tween20, 10% BSA, 1% fish gelatine, diluted in PBS, pH 7.4 and incubated overnight at 4 C with anti-Nrf2 antibody (GeneTex, GTX103322) diluted in blocking solution. After washing with PBS, sections were exposed to biotinylated secondary goat anti-rabbit antibody diluted in blocking solution for 1h at RT, followed by Alexa Fluor 488 conjugated Streptavidin (Thermo Fisher Scientific, s11223) for 30min at RT. In the next step, sections were incubated overnight at 4°C with the appropriate primary antibody diluted in blocking solution. Primary antibodies and dilutions used in the study are given in Table 3. After washing, sections were incubated with an Alexa Fluor 594 conjugated secondary donkey anti-goat or goat anti-mouse antibody diluted in blocking solution for 1h. Secondary antibodies and dilutions used are given in Table 4. Sections were counterstained with Hoechst 33342 (Invitrogen, 1:10000) to visualize cell nuclei. Stained sections were examined and photographed with a Nikon ECLIPSE 80i microscope and 40x objective. Quantification of axonal damage, oligodendrocytes and microglia was performed by counting amyloid precursor protein (APP) positive bulbs, oligodendrocyte transcription factor (Olig2)-positive cells and ionized calcium-binding adapter molecule 1 (Iba1)–positive cells, respectively. Two brain slices from region 235 and two slices from region 265 from each animal were used for analysis. Counting was performed by at least two independent examiners in a blinded manner. Results were expressed as number of cells/mm^2.

For LFB staining, sections were deparaffinized and hydrated, then incubated in a 0.1% LFB solution overnight at 56 °C. The next day, the excess of staining solution was rinsed off in 95% ethyl alcohol,

washed in distilled water and differentiated in 0.05% lithium carbonate solution for 20 s. After this, PAS staining was performed by oxidizing the slides in 0.5% periodic acid solution for 5 min, rinsing it in distilled water, and incubating it in Schiff reagent for 15 min. Afterwards, sections were washed in tap water for 5 min. Slides were cpounterstained with Mayer's hematoxylin for 1 min. The tissue was then washed again, dehydrated and mounted in DPX.

Statistics

If not stated otherwise, at least two experimental settings were performed with a group size of ≥ 3 animals each per experiment and experimental group (n ≥ 6). Equal variances and normal distribution were checked by the Bartlett test and the Shapiro-Wilk test respectively. Intergroup differences of parametric data were tested either by Student's t-test (comparison of two groups) or ANOVA (multiple comparisons), followed by Tukey's or Bonferroni post hoc tests using GraphPad Prism 5 (GraphPad Software), if not stated otherwise. All data are given as arithmetic means ± SEM. The p values are indicated as *p ≤ 0.05, **p ≤ 0.01, ***p ≤ 0.001. For further information, see figure legends.

Results

Oxidative stress during early cuprizone intoxication

We recently performed genome wide gene expression studies of early cuprizone intoxication (i.e. 2 days) to gain a deeper understanding of the biochemical pathways activated in response to cuprizone intoxication (Krauspe et al. 2015). In this study, we re-evaluated these data with respect to oxidative stress reactions and defense mechanisms. As listed in table 1, in 14 gene enrichments related to oxidative stress responses between 12.8% and 60.0% of the genes belonging to these gene ontologies showed a significantly altered mRNA expression profile ($p < 0.05$, FC > 1.25) in the corpus callosum of cuprizone-fed animals. These results indicate the critical role of oxidative stress in early lesion development after cuprizone intoxication. The complete list of all regulated genes belonging to the selected gene ontologies is summarized in the supplementary table 1. To confirm our gene expression array data at a later time point (i.e. 1 week) and to further investigate, whether the Nrf2/ARE system is indeed activated in early demyelinating lesions, RT-qPCR for the following genes was performed: heme oxigenase (Hmox1), glutamate-cysteine ligase, catalytic subunit (GCLC) and thioredoxin reductase (TxnRD1) (figure 1). The expression of these genes is typically regulated by Nrf2-binding to the ARE (Brown and Drake 1973; Clovis and Hargreaves 1988; Patenaude et al. 2005). Gene expression of all three genes was significantly induced after one week cuprizone intoxication indicating the functional relevance of Nrf2-signaling in the initial oligodendrocyte-stress process within the corpus callosum.

Activation of the Nrf2/ARE system during early cuprizone intoxication

To further investigate the temporal and quantitative pattern of Nrf2/ARE-activation, we decided to include transgenic ARE-Luc mice in this study. Among ARE-activation, these mice express a functionally active luciferase protein (originates from the firefly, *lat. photinus pyralis*). In this approach, the luciferase activity directly correlates with Nrf2-activity. Luminescence can thereby be used as a sufficient measure for Nrf2-activity. Animals were fed cuprizone for up to one week and the luciferase-activity was measured on a daily basis *in vivo*. Mice fed normal chow served as controls. Summarized and normalized data of all experiments is shown in figure 2A. A significant induction of luciferase-activity was observed in cuprizone-fed mice as early as two days of cuprizone intoxication, indicating a functional role of Nrf2-activity, at least at this lesion stage. Representative images of the *in vivo* bioluminescence analysis using the XENOGEN living image system are depicted in the upper row of figure 2B. By setting appropriate ROIs, these measurements were used for quantification. Since the *in vivo* measurement does not allow a statement about regional differences in ARE activation, animals were sacrificed at the end of the experiment, frontal brain sections prepared, and a luminescence measurement conducted. Representative images are shown in figure 2C. These

experiments revealed the highest luminescence signal within the corpus callosum (CC) white matter tract, a region which is particularly vulnerable to cuprizone intoxication and therefore one of the best studied brain regions in this animal model.

Cellular source of Nrf2 in the cuprizone model

In a next set of experiments, we aimed to identify the expression pattern and cellular source of Nrf2 in response to cuprizone intoxication. As shown in figure 3A, the number of Nrf2-positive cells increased in both 1 and 3 weeks cuprizone groups. Double-staining against Nrf2 and GFAP revealed that Nrf2-positive astrocytes were present at very low numbers in all investigated groups (figure 3B), indicating, low stress levels of astrocytes, even due cuprizone-intoxication. In contrast, the number of Nrf2-positive oligodendrocytes markedly increased within the CC white matter in both 1 and 3 weeks treated animals (figure 3C).

Over-activation of the astrocytic Nrf2/ARE system protects against cuprizone toxicity

So far we were able to demonstrate that oxidative stress is a characteristic feature of early cuprizone-induced lesions which is paralleled by the activation of the Nrf2/ARE pathway in oligodendrocytes. However, since cuprizone induces profound demyelination in a matter of weeks, the activation of the Nrf2/ARE pathways has to be considered as insufficient to overcome deleterious effects and act as a protective cellular response. We therefore decided to strengthen this archetypical cytoprotective pathway by comparing the outcome of wt and Keap1-KO mice after a prolonged, 3 weeks cuprizone challenge. Since astrocytes are critically involved in the maintenance of redox homeostasis in the brain (Schreiner et al. 2015), Keap1 was deleted specifically in this macroglia cell population which results in a genetic model for constitutive activation of the Nrf2/ARE pathway in astrocytes.

In wild type animals, cuprizone intoxication induced the loss of myelin (visualized by luxol fast blue-stains, LFB, figure 4A, 1st row) and oligodendrocytes (visualized by anti-Olig2 staining, figure 4A, 2nd row), microgliosis (visualized by anti-Iba1 staining, figure 4A, 3rd row) and acute axonal damage (APP+-spheroids, red arrows, figure 4A, 4th row) (Clarner et al. 2015). In sharp contrast, the loss of myelin and oligodendrocytes was almost completely prevented in Keap1-KO mice (figure 4A, 3rd column). Furthermore, the number of microglia cells within the CC was significantly lower in comparison to treated wild type animals. Histological quantifications of oligodendrocytes, microglia and APP+-spheroids numbers are shown in figure 4B. These results demonstrate that strengthening of the Nrf2 system in astrocytes is sufficient to prevent or delay the development of demyelinating lesions, neuroinflammation and axonal damage.

Astrocyte reactivity is unchanged in Keap1-KO mice

A characteristic feature of both MS lesions and cuprizone-induced lesions is the accumulation of reactive astrocytes within the damaged CNS areas (Clarner et al. 2012). In a next set of experiments, we therefore investigated the activation of astroglia in wild type as well as Keap1-KO mice after cuprizone intoxication. Data are presented in figure 5. As expected, cuprizone exposure significantly increased GFAP+ cell numbers in the CC (figures 5A and B). Despite the above mentioned amelioration of cuprizone toxicity, the increase in astrocyte numbers within the CC was comparable in both mouse strains and not abolished or dampened in Keap1-KO mice. Since a critical molecule which is secreted by activated astrocytes and involved in the activation of local microglia in the cuprizone model is the chemokine CXCL10 (Clarner et al. 2015), we used the expression of CXCL10 mRNA as an indirect indicator to asses astrocyte reactivity. As shown in figure 5B and in accordance with previous studies (Clarner et al. 2015), cuprizone administration resulted in a significant increase of CXCL10 expression. This induction was comparable in Keap1-KO mice.

Discussion

In the present study, we demonstrate that cuprizone intoxication induces the Nrf2/ARE system in the CC and that the genetic hyper-activation of astrocytic Nrf2 is sufficient to prevent oligodendrocyte loss, microgliosis and axonal damage without affecting astroglial activation in a demyelinating animal model. Further, we provide a set of cuprizone-dependent oxidative stress-related genes regulated within the CC.

Relevance of the cuprizone model for studying Nrf2-signaling and neuroinflammation

Neuroinflammation is defined as the brain's activation of the innate immune system due to external stimuli or brain-intrinsic responses to injuries. Its main function is to protect the CNS and neuronal circuits from degeneration and damage and to take care of brain homeostasis under deleterious conditions. It is well-established that innate immune responses of the brain are actively involved in the origin and progression of neurological diseases and disorders (Spencer et al. 2012; Zhang and Jiang 2015). Besides other acute CNS responses to such threatening conditions, oxidative stress reactions driven by neuroinflammation and the production of ROS and RNS in activated microglia play a critical role in the propagation of demyelination and neurodegeneration (Gonsette 2008; Haider et al. 2011; Licht-Mayer et al. 2015; Wang et al. 2014). Nrf2 activation is a highly conserved adaptive mechanism of eukaryotic cells to prevent oxidative stress and is a well-documented phenomenon in MS lesions (Licht-Mayer et al. 2015). The induction of Nrf2 and it`s target genes (i.e. Hmox1) has been demonstrated in oligodendrocytes in initial white matter lesions (Licht-Mayer et al. 2015). In contrast, Nrf2-positive astrocytes and macrophages were mainly found in later stages of

active lesions (Licht-Mayer et al. 2015). Our findings on 1 and 3 week old cuprizone-induced lesions confirm the presence of high numbers of Nrf2-positive oligodendrocytes during the active development of demyelinated lesions. Further studies on the cuprizone model will have to show weather the number of Nrf2-positive astrocytes increases in chronically demyelinated lesions in the cuprizone model (i.e. 13 weeks cuprizone intoxication).

Our findings indicate an early oligodendrocyte-mediated defense attempt against oxidative stress via the functional induction of Nrf2. However, this attempt obviously fails to prevent neuroinflammation and the loss of oligodendrocytes. Faster (i.e. during the first stages of lesion formation) activation of astroglial Nrf2 by pharmacological interventions therefore might help to prevent lesion progression.

Although the pathological mechanisms of cuprizone fundamentally differ from neurological diseases such as MS, it perfectly mimics basic mechanisms of brain-intrinsic inflammation and subsequent axonal damage. With respect to Nrf2-activation, we show herein that during initial cuprizone-intoxication, the Nrf2 system gets activated within the damaged areas such as the CC, whereas the cortical grey matter showed lower Nrf2-activity. However, similar to the human situation, this potentially protective attempt fails to rescue oligodendrocytes and to prevent demyelination in wild type animals.

Regarding the source of free radicals in the cuprizone model, Liu and colleagues recently identified microglia as important producers of ROS in this model. Furthermore, they describe the microglial Hv1 channel as a key factor for this ROS-production (Liu et al. 2015).

Until today, it is not completely clear why oligodendrocytes are selectively vulnerable to cuprizone intoxication. However, the mechanism by which cuprizone is thought to unfold its toxicity is via disturbing both mitochondrial functions as well as important detoxifying enzymes such as superoxide dismutase (Faizi et al. 2016). Oligodendrocytes, in contrast to other glia cells, display a high metabolic activity and membrane synthesis rate under physiological conditions. A high ATP-synthesis rate causes the formation of hydrogen peroxide as a toxic byproduct, therefore leading to elevated oxidative burden. Furthermore, they have only low concentrations of the anti-oxidative enzyme glutathione (Thorburne and Juurlink 1996), making them more susceptible to both intrinsic and extrinsic (i.e. microglia-derived) oxidative challenge. Here, we can show that cuprizone indeed seems to selectively induce Nrf2 in oligodendrocytes, indicating early and selective oxidative stress in this cell type.

Taken together, cuprizone-intoxication is a helpful tool to study basic mechanisms of oligodendrocyte loss, neuroinflammation, oxidative stress and Nrf2-activation.

The role of the astrocytic Nrf2/ARE system for neuroinflammation

Astrocytes possess a variety of roles in maintaining an optimally suited milieu for neuronal function, among the maintenance of redox potential (Zhang and Jiang 2015). In the presence of an insult however, astrocytes amplify the inflammatory process that is initiated by microglia (Crotti and Glass 2015; Saijo et al. 2009). The importance of (dysfunctional) astrocytes for the propagation of inflammation has been well demonstrated for distinct neurological diseases such as Alzheimer`s, Alexander`s and Huntington`s disease (Crotti and Glass 2015; Olabarria et al. 2015; Zhang and Jiang 2015). Astrocytes produce chemokines such as CXCL1, CCL2, CXCL10 or CCL11 that influence microglia reactivity (Clarner et al. 2015; Hennessy et al. 2015; Parajuli et al. 2015). Another well-described mechanism by which microglia get activated is via increased tissue levels of ROS (Ishihara et al. 2015; Liu et al. 2015; Qiu et al. 2015). Reduced concentrations of ROS therefore might efficiently inhibit neuroinflammation. Here, we provide evidence that the consistent hyperactivation of Nrf2 signaling in astrocytes prevents the formation and progression of demyelinated lesions. Furthermore, the number of astrocytes and the induction of CXCL10 were unchanged in Keap1-KO mice. Therefore, the most obvious hypothesis explaining our results is that hyperactivated Nrf2 leads to enhanced detoxification of radicals within the tissue, thereby inhibiting neuroinflammation and protecting oligodendrocytes and axons. Future studies will have to analyze the levels of ROS/RNS within the brain of cuprizone-fed Keap1-KO animals.

A less obvious but fully relevant hypothesis to explain our results is that Nrf2-dependent changes in the release of anti-inflammatory mediators might influence the reactivity and diversification of microglia. So far, not much is known about the Nrf2-triggered production of such mediators in the brain. To address this important point, a detailed bioinformatics approach, both *in vitro* and *in vivo* (gene arrays and pathway analysis), could help to elucidate the role of Nrf2-signalling for modulating the interplay of different glial cell types.

In summary, our data clearly demonstrate that the astrocyte-specific activation of Nrf2 is sufficient to prevent the formation of demyelinating lesions and neuroinflammation in a non-autoimmune- driven MS model. The identification of the underlying mechanisms that regulate these processes are of upmost importance to (A) gain a deeper understanding of MS lesion progression and (B) to develop novel therapeutic strategies.

Figure legends

Table 1 Oxidative stress responses in the cuprizone model

Affymetrix gene array data of 1 week cuprizone-fed wild type animals are shown. Gene ontologies related to oxidative stress and defenses are shown. More detailed information including gene symbols of regulated genes are given in the supplementary table 1.

Figure 1 Nrf2-target gene expression in the cuprizone model.

Array results were confirmed in additional animals after 1 week cuprizone treatment by RT-qPCR. Results for Hmox1 (heme oxygenase), GCLC (glutamate-cysteine ligase, catalytic subunit) and TxnRD1 (Thioredoxin reductase 1) are shown (n=6).

*p <0.05; **p<0.01, ***p<0.001.

Figure 2 Cuprizone induces Nrf2-activity in the mouse brain.

(A) Shows the cumulative results of luminescence intensity measured *in vivo* in luc-ARE mice fed cuprizone or normal chow for 1 week. (B) shows representative examples of these measurements. Higher luminescence intensity indicates induced Nrf2 activity in the brain.. (C) *Ex vivo* analysis at the end of the experiment showed highest luminescence signal within the CC, a region especially vulnerable to cuprizone intoxication. *p <0.05; **p<0.01

Figure 3 Cuprizone intoxication increases Nrf2-activation in oligodendrocytes

In (A), results of an immunohistochemical staining against Nrf2 of control animals and animals fed cuprizone for 1 and 3 weeks are shown. Staining-intensity against Nrf2 increased with feeding cuprizone. (B) and (C) display double stainings against Nrf2 and the cellular markers GFAP and Olig2. Oligodendrocytes can clearly be identified as the main responsive cells to cuprizone-intoxication with respect to Nrf2-accumulation within the cell. Only very low numbers of Nrf2-positive astrocytes were observed.

Figure 4 Nrf2 hyperactivation ameliorates cuprizone toxicity

In (A), typical (immuno-)histochemical results of control animals and animals fed cuprizone for 3 weeks are shown. Myelin staining intensity loss (LFB) was markedly reduced within the CC of cuprizone-fed Keap1-KO animals. Furthermore, the numbers of Olig2-positive cells were higher, whereas microgliosis and the accumulation of APP+ bulbs were less severe in Keap1-KO mice compared to wild type animals. In (B), quantifications of cell numbers and APP+ bulbs within the CC

are shown. Scale bars: 150µm in the upper row; 50µm in lower rows. *p <0.05; **p<0.01; ***p<0.001

Figure 5 Astrocyte responses are unchanged in Keap1-KO mice

The increase of astrocyte numbers did not differ between cuprizone-fed wild type and Keap1-KO mice after 3 weeks. Representative pictures of GFAP-staining are shown in (A). Quantification of cell numbers (B) did reveal a comparable increase in cell numbers in both genotypes compared to mice receiving normal show. The expression of astrocyte-derived chemokine CXCL10 did not differ in both genotypes, indicating similar pro-inflammatory astrocytic responses. Scale bar: 50µm; *p <0.05; **p<0.01; ***p<0.001

Supplementary table 1. Selected gene ontologies related to oxidative stress and defense

Gene expression was analyzed using the GeneChip® Mouse Gene 1.0 ST Array (Affymetrix, Santa Clara, CA, USA) in independent triplicates. Total RNA was isolated and quantified from the CC (Nanodrop). RNA quality was assessed as published (Krauspe et al. 2015) and probes prepared and hybridized according to the Ambion whole-transcript expression and the Affymetrix whole-transcript terminal labelling and control kit manuals. For a more detailed protocol see (Krauspe et al. 2015).

References

Al-Sawaf O, Clarner T, Fragoulis A, Kan YW, Pufe T, Streetz K, Wruck CJ. 2015. Nrf2 in health and disease: current and future clinical implications. Clin Sci (Lond) 129:989-99.

Bajenaru ML, Zhu Y, Hedrick NM, Donahoe J, Parada LF, Gutmann DH. 2002. Astrocyte-specific inactivation of the neurofibromatosis 1 gene (NF1) is insufficient for astrocytoma formation. Mol Cell Biol 22:5100-13.

Brown RE, Drake RM. 1973. Letter: Antilipolytic therapy and the respiratory-distress syndrome. Lancet 302:1021.

Chen H, Assmann JC, Krenz A, Rahman M, Grimm M, Karsten CM, Kohl J, Offermanns S, Wettschureck N, Schwaninger M. 2014. Hydroxycarboxylic acid receptor 2 mediates dimethyl fumarate's protective effect in EAE. J Clin Invest 124:2188-92.

Clarner T, Diederichs F, Berger K, Denecke B, Gan L, van der Valk P, Beyer C, Amor S, Kipp M. 2012. Myelin debris regulates inflammatory responses in an experimental demyelination animal model and multiple sclerosis lesions. Glia 60:1468-80.

Clarner T, Janssen K, Nellessen L, Stangel M, Skripuletz T, Krauspe B, Hess FM, Denecke B, Beutner C, Linnartz-Gerlach B and others. 2015. CXCL10 triggers early microglial activation in the cuprizone model. J Immunol 194:3400-13.

Clarner T, Wieczorek N, Krauspe B, Jansen K, Beyer C, Kipp M. 2014. Astroglial redistribution of aquaporin 4 during spongy degeneration in a Canavan disease mouse model. J Mol Neurosci 53:22-30.

Clovis J, Hargreaves JA. 1988. Fluoride intake from beverage consumption. Community Dent Oral Epidemiol 16:11-5.

Crotti A, Glass CK. 2015. The choreography of neuroinflammation in Huntington's disease. Trends Immunol 36:364-73.

Dang J, Brandenburg LO, Rosen C, Fragoulis A, Kipp M, Pufe T, Beyer C, Wruck CJ. 2012. Nrf2 expression by neurons, astroglia, and microglia in the cerebral cortical penumbra of ischemic rats. J Mol Neurosci 46:578-84.

Dohlen G, Odland HH, Carlsen H, Blomhoff R, Thaulow E, Saugstad OD. 2008. Antioxidant activity in the newborn brain: a luciferase mouse model. Neonatology 93:125-31.

Faizi M, Salimi A, Seydi E, Naserzadeh P, Kouhnavard M, Rahimi A, Pourahmad J. 2016. Toxicity of cuprizone a Cu(2+) chelating agent on isolated mouse brain mitochondria: a justification for demyelination and subsequent behavioral dysfunction. Toxicol Mech Methods 26:276-83.

Fet N, Alizai PH, Fragoulis A, Wruck C, Pufe T, Tolba RH, Neumann UP, Klinge U. 2014. In vivo characterisation of the inflammatory reaction following mesh implantation in transgenic mice models. Langenbecks Arch Surg 399:579-88.

Fragoulis A, Laufs J, Muller S, Soppa U, Siegl S, Reiss LK, Tohidnezhad M, Rosen C, Tenbrock K, Varoga D and others. 2012. Sulforaphane has opposing effects on TNF-alpha stimulated and unstimulated synoviocytes. Arthritis Res Ther 14:R220.

Frischer JM, Bramow S, Dal-Bianco A, Lucchinetti CF, Rauschka H, Schmidbauer M, Laursen H, Sorensen PS, Lassmann H. 2009. The relation between inflammation and neurodegeneration in multiple sclerosis brains. Brain 132:1175-89.

Gillard GO, Collette B, Anderson J, Chao J, Scannevin RH, Huss DJ, Fontenot JD. 2015. DMF, but not other fumarates, inhibits NF-kappaB activity in vitro in an Nrf2-independent manner. J Neuroimmunol 283:74-85.

Goldberg J, Clarner T, Beyer C, Kipp M. 2015. Anatomical Distribution of Cuprizone-Induced Lesions in C57BL6 Mice. J Mol Neurosci 57:166-75.

Gonsette RE. 2008. Neurodegeneration in multiple sclerosis: the role of oxidative stress and excitotoxicity. J Neurol Sci 274:48-53.

Groebe A, Clarner T, Baumgartner W, Dang J, Beyer C, Kipp M. 2009. Cuprizone treatment induces distinct demyelination, astrocytosis, and microglia cell invasion or proliferation in the mouse cerebellum. Cerebellum 8:163-74.

Haider L, Fischer MT, Frischer JM, Bauer J, Hoftberger R, Botond G, Esterbauer H, Binder CJ, Witztum JL, Lassmann H. 2011. Oxidative damage in multiple sclerosis lesions. Brain 134:1914-24.

Hennessy E, Griffin EW, Cunningham C. 2015. Astrocytes Are Primed by Chronic Neurodegeneration to Produce Exaggerated Chemokine and Cell Infiltration Responses to Acute Stimulation with the Cytokines IL-1beta and TNF-alpha. J Neurosci 35:8411-22.

Huang Y, Li W, Su ZY, Kong AT. 2015. The complexity of the Nrf2 pathway: beyond the antioxidant response. J Nutr Biochem.

Ishihara Y, Takemoto T, Itoh K, Ishida A, Yamazaki T. 2015. Dual Role of Superoxide Dismutase 2 Induced in Activated Microglia: OXIDATIVE STRESS TOLERANCE AND CONVERGENCE OF INFLAMMATORY RESPONSES. J Biol Chem 290:22805-17.

Johnson DA, Amirahmadi S, Ward C, Fabry Z, Johnson JA. 2010. The absence of the pro-antioxidant transcription factor Nrf2 exacerbates experimental autoimmune encephalomyelitis. Toxicol Sci 114:237-46.

Johnson DA, Johnson JA. 2015. Nrf2-a therapeutic target for the treatment of neurodegenerative diseases. Free Radic Biol Med:FRBMD1500535.

Kim W, Zandona ME, Kim SH, Kim HJ. 2015. Oral disease-modifying therapies for multiple sclerosis. J Clin Neurol 11:9-19.

Kipp M, Clarner T, Dang J, Copray S, Beyer C. 2009. The cuprizone animal model: new insights into an old story. Acta Neuropathol 118:723-36.

Krauspe BM, Dreher W, Beyer C, Baumgartner W, Denecke B, Janssen K, Langhans CD, Clarner T, Kipp M. 2015. Short-term cuprizone feeding verifies N-acetylaspartate quantification as a marker of neurodegeneration. J Mol Neurosci 55:733-48.

Lassmann H. 2014. Multiple sclerosis: lessons from molecular neuropathology. Exp Neurol 262 Pt A:2-7.

Licht-Mayer S, Wimmer I, Traffehn S, Metz I, Bruck W, Bauer J, Bradl M, Lassmann H. 2015. Cell type-specific Nrf2 expression in multiple sclerosis lesions. Acta Neuropathol 130:263-77.

Linker RA, Lee DH, Ryan S, van Dam AM, Conrad R, Bista P, Zeng W, Hronowsky X, Buko A, Chollate S and others. 2011. Fumaric acid esters exert neuroprotective effects in neuroinflammation via activation of the Nrf2 antioxidant pathway. Brain 134:678-92.

Liu J, Tian D, Murugan M, Eyo UB, Dreyfus CF, Wang W, Wu LJ. 2015. Microglial Hv1 proton channel promotes cuprizone-induced demyelination through oxidative damage. J Neurochem 135:347-56.

Liu JS, Zhao ML, Brosnan CF, Lee SC. 2001. Expression of inducible nitric oxide synthase and nitrotyrosine in multiple sclerosis lesions. Am J Pathol 158:2057-66.

Lu F, Selak M, O'Connor J, Croul S, Lorenzana C, Butunoi C, Kalman B. 2000. Oxidative damage to mitochondrial DNA and activity of mitochondrial enzymes in chronic active lesions of multiple sclerosis. J Neurol Sci 177:95-103.

Mahad DH, Trapp BD, Lassmann H. 2015. Pathological mechanisms in progressive multiple sclerosis. Lancet Neurol 14:183-193.

Mena MA, Garcia de Yebenes J. 2008. Glial cells as players in parkinsonism: the "good," the "bad," and the "mysterious" glia. Neuroscientist 14:544-60.

Offermanns S, Schwaninger M. 2015. Nutritional or pharmacological activation of HCA(2) ameliorates neuroinflammation. Trends Mol Med 21:245-55.

Okawa H, Motohashi H, Kobayashi A, Aburatani H, Kensler TW, Yamamoto M. 2006. Hepatocyte-specific deletion of the keap1 gene activates Nrf2 and confers potent resistance against acute drug toxicity. Biochem Biophys Res Commun 339:79-88.

Olabarria M, Putilina M, Riemer EC, Goldman JE. 2015. Astrocyte pathology in Alexander disease causes a marked inflammatory environment. Acta Neuropathol 130:469-86.

Parajuli B, Horiuchi H, Mizuno T, Takeuchi H, Suzumura A. 2015. CCL11 enhances excitotoxic neuronal death by producing reactive oxygen species in microglia. Glia 63:2274-84.

Patenaude A, Murthy MR, Mirault ME. 2005. Emerging roles of thioredoxin cycle enzymes in the central nervous system. Cell Mol Life Sci 62:1063-80.

Qiu LL, Ji MH, Zhang H, Yang JJ, Sun XR, Tang H, Wang J, Liu WX, Yang JJ. 2015. NADPH oxidase 2-derived reactive oxygen species in the hippocampus might contribute to microglial activation in postoperative cognitive dysfunction in aged mice. Brain Behav Immun.

Saijo K, Winner B, Carson CT, Collier JG, Boyer L, Rosenfeld MG, Gage FH, Glass CK. 2009. A Nurr1/CoREST pathway in microglia and astrocytes protects dopaminergic neurons from inflammation-induced death. Cell 137:47-59.

Schreiner B, Romanelli E, Liberski P, Ingold-Heppner B, Sobottka-Brillout B, Hartwig T, Chandrasekar V, Johannssen H, Zeilhofer HU, Aguzzi A and others. 2015. Astrocyte Depletion Impairs Redox Homeostasis and Triggers Neuronal Loss in the Adult CNS. Cell Rep 12:1377-84.

Schuh C, Wimmer I, Hametner S, Haider L, Van Dam AM, Liblau RS, Smith KJ, Probert L, Binder CJ, Bauer J and others. 2014. Oxidative tissue injury in multiple sclerosis is only partly reflected in experimental disease models. Acta Neuropathol 128:247-66.

Sharma R, Fischer MT, Bauer J, Felts PA, Smith KJ, Misu T, Fujihara K, Bradl M, Lassmann H. 2010. Inflammation induced by innate immunity in the central nervous system leads to primary astrocyte dysfunction followed by demyelination. Acta Neuropathol 120:223-36.

Slowik A, Schmidt T, Beyer C, Amor S, Clarner T, Kipp M. 2015. The sphingosine 1-phosphate receptor agonist FTY720 is neuroprotective after cuprizone-induced CNS demyelination. Br J Pharmacol 172:80-92.

Spencer JP, Vafeiadou K, Williams RJ, Vauzour D. 2012. Neuroinflammation: modulation by flavonoids and mechanisms of action. Mol Aspects Med 33:83-97.

Spray ESD. 2011. Astrocytes: Wiring the brain: CRC Press.

Thorburne SK, Juurlink BH. 1996. Low glutathione and high iron govern the susceptibility of oligodendroglial precursors to oxidative stress. J Neurochem 67:1014-22.

van Horssen J, Schreibelt G, Drexhage J, Hazes T, Dijkstra CD, van der Valk P, de Vries HE. 2008. Severe oxidative damage in multiple sclerosis lesions coincides with enhanced antioxidant enzyme expression. Free Radic Biol Med 45:1729-37.

Wang P, Xie K, Wang C, Bi J. 2014. Oxidative stress induced by lipid peroxidation is related with inflammation of demyelination and neurodegeneration in multiple sclerosis. Eur Neurol 72:249-54.

Wruck CJ, Fragoulis A, Gurzynski A, Brandenburg LO, Kan YW, Chan K, Hassenpflug J, Freitag-Wolf S, Varoga D, Lippross S and others. 2011. Role of oxidative stress in rheumatoid arthritis: insights from the Nrf2-knockout mice. Ann Rheum Dis 70:844-50.

Wruck CJ, Gotz ME, Herdegen T, Varoga D, Brandenburg LO, Pufe T. 2008. Kavalactones protect neural cells against amyloid beta peptide-induced neurotoxicity via extracellular signal-regulated kinase 1/2-dependent nuclear factor erythroid 2-related factor 2 activation. Mol Pharmacol 73:1785-95.

Zhang F, Jiang L. 2015. Neuroinflammation in Alzheimer's disease. Neuropsychiatr Dis Treat 11:243-56.

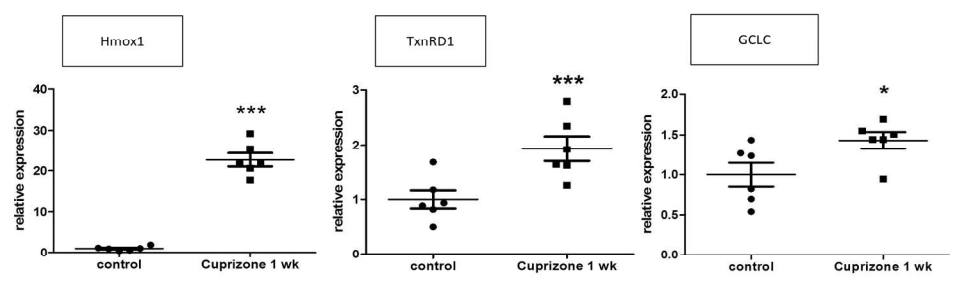Figure 1
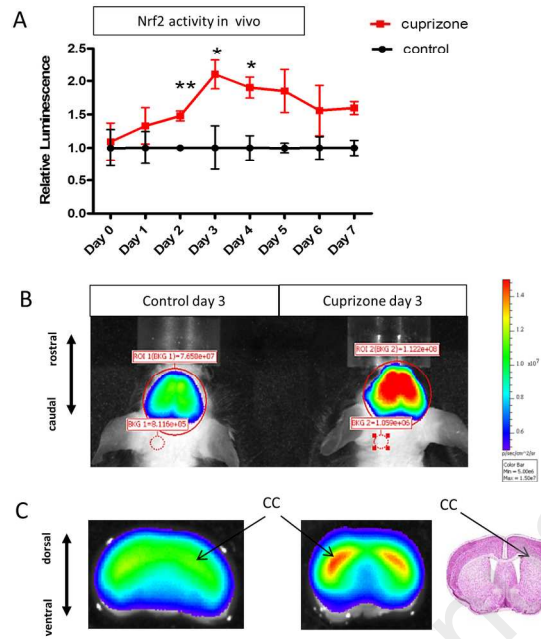
190x142mm (300 x 300 DPI)

Figure 2

190x142mm (300 x 300 DPI)

Figure 3

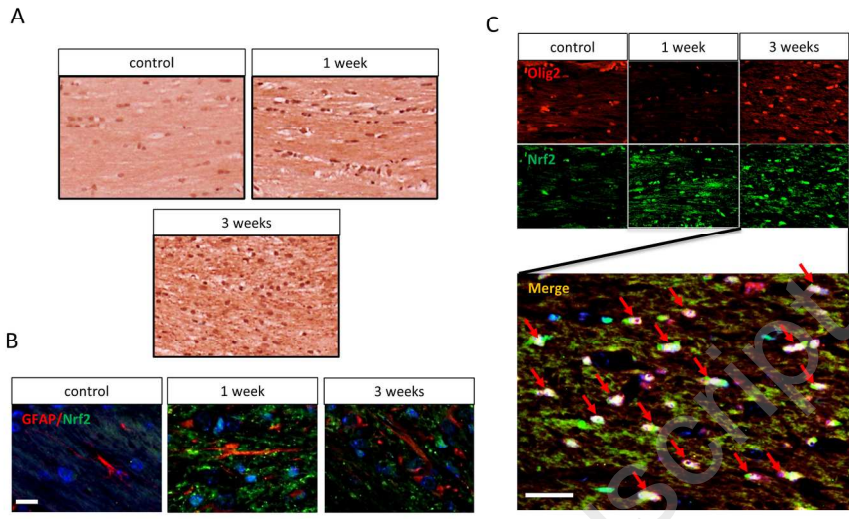190x142mm (300 x 300 DPI)
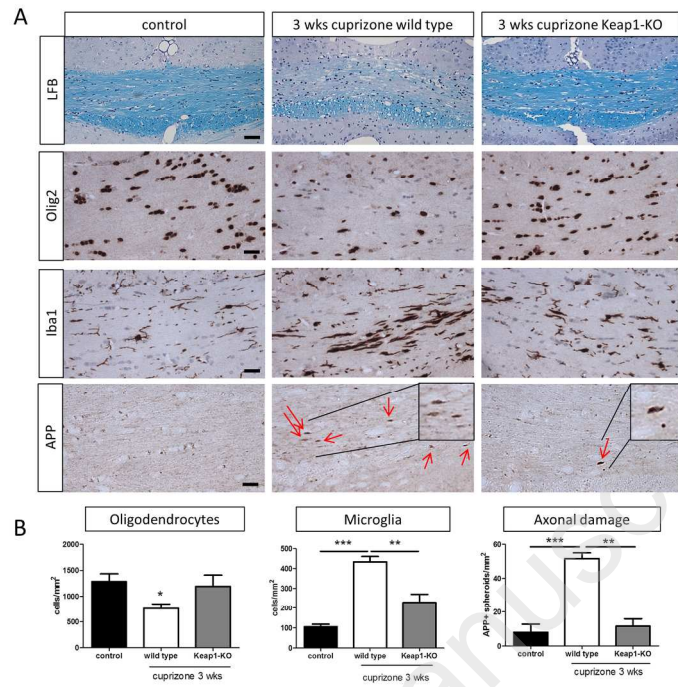
Figure 4

190x142mm (300 x 300 DPI)

A

B
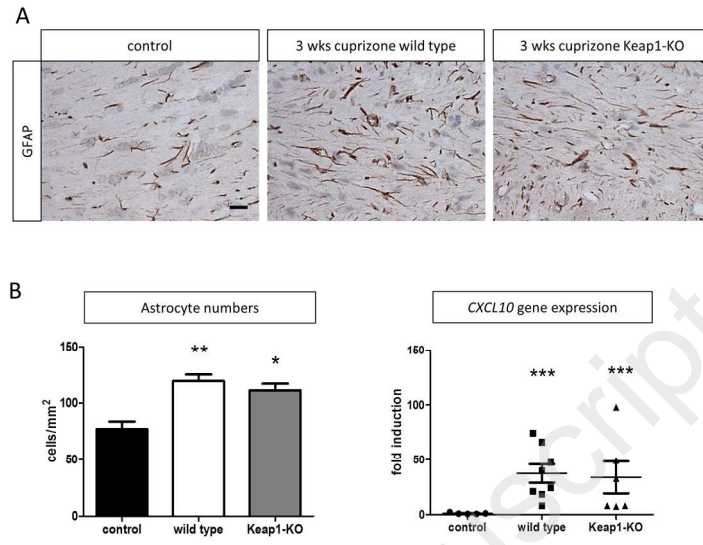
Figure 5

190x142mm (300 x 300 DPI)

ID	Name	Number Changed	Changed (%)	Z Score
GO:0016717	oxidoreductase activity, acting on paired donors, with oxidation of a pair of donors resulting in the reduction of molecular oxygen to two molecules of water	6	60.00	5.7326
GO:0016645	oxidoreductase activity, acting on the CH-NH group of donors	9	34.62	4.6660
GO:0016175	superoxide-generating NADPH oxidase activity	3	37.50	2.8757
GO:0016835	carbon-oxygen lyase activity	11	18.33	2.6266
GO:0016628	oxidoreductase activity, acting on the CH-CH group of donors, NAD or NADP as acceptor	5	25.00	2.5701
GO:0016491	oxidoreductase activity	95	12.79	3.9571
GO:2000377	regulation of reactive oxygen species metabolic process	15	30.00	5.3186
GO:0000302	response to reactive oxygen species	22	20.95	4.4302
GO:0070482	response to oxygen levels	35	15.70	3.6830
GO:0050665	hydrogen peroxide biosynthetic process	3	42.86	3.1914
GO:0060263	regulation of respiratory burst	3	37.50	2.8757
GO:0045730	respiratory burst	3	37.50	2.8757
WP1496	oxidative damage	13	30.95	3.6021
MP:0005388	respiratory system phenotype	157	14.08	2.0718

Table 1: Gene ontologies related to oxidative stress and numbers of changed genes in response to short-term cuprizone exposure

Name	Forward Sequence	Reverse Sequence
Gclc	GGGGTGACGAGGTGGAGTA	GTTGGGGTTTGTCCTCTCCC
Hmox1	AAGCCGAGAATGCTGAGTTCA	GCCGTGTAGATATGGTACAAGGA
Txnrd1	GGGCTTCCACGTGCTGGGTC	TCCCCCAGAGCGCTTCGTCA
CXCL10	CCAAGTGCTGCCGTCATTTTC	GGCTCGCAGGGATGATTTCAA
HPRT (reference gene)	GCTGGTGAAAAGGACCTCT	CACAGGACTAGAACACCTGC

Table 2 Primer sequences used for RT-qPCR

Antibody	Host	protein	Dilution	AG Retrival	Supplier Catalogue No.
APP	mouse	Amyloid precursor protein	1:5000	10' Tris/EDTA	Millipore, MAB 348
IBA1	rabbit	Ionized calcium-binding adaptor molecule (microglia/macrophages)	1:10000	10' Tris/EDTA	Wako, 019-19741
Olig2	rabbit	Oligodendrocyte transcription factor 2	1:2000	Tris/EDTA	Millipore, AB9610
Olig2	mouse	Oligodendrocyte transcription factor 2	1:1000	20' Citrate	Millipore, MABN50
GFAP	rabbit	Glial fibrillary acidic protein	1:1000	Tris/EDTA	Encore, RPCA-GFAP
GFAP	goat	Glial fibrillary acidic protein	1:100	20' Citrate	Santa Cruz, sc6170
NRF2	rabbit	Nuclear factor erythroid 2-related factor 2	1:100	20' Citrate	GeneTex, GTX103322

Table 3 Primary antibodies used in this study

Antibody	Host	Directed against	Dilution	Supplier Catalogue No.
Biotinylated anti-mouse IgG	Horse	Secondary Ab against mouse IgGs	1:50	Vector Laboratories BA-2000
Biotinylated anti-rabbit IgG	Goat	Secondary Ab against rabbit IgGs	1:50	Vector Laboratories BA-1000
594 fluorescent anti-mouse IgG	Goat	Secondary Ab against mouse IgGs	1:500	Life Technologies, A11032
594 fluorescent anti-goat IgG	Donkey	Secondary Ab against goat IgGs	1:500	Life Technologies, A11058

Table 4 Secondary antibodies used in this study

ID	Name	Ontology Type	Number Changed	Number Measured	Number in Gene-Set	Percent Changed	Percent Present	Z Score	FisherExactP	gene symbols
GO:0016717	oxidoreductase activity, acting on paired donors, with oxidation of a pair of donors resulting in the reduction of molecular oxygen to two molecules of water	MF	6	10	10	60	100	5,7326	0,0001	4833423E24Rik|Fads3|Sc5d|Scd1|Scd2|Scd3
GO:0016645	oxidoreductase activity, acting on the CH-NH group of donors	MF	9	26	27	34,62	96,3	4,666	0,0002	Aldh1l1|Aldh1l2|Dhfr|Mthfd2|Pipox|Prodh|Pycr1|Qdpr|Sardh
GO:0016175	superoxide-generating NADPH oxidase activity	MF	3	8	8	37,5	100	2,8757	0,0269	Cyba|Cybb|Ncf1
GO:0016835	carbon-oxygen lyase activity	MF	11	60	60	18,33	100	2,6266	0,0182	Agxt2l1|Alkbh1|Car12|Car14|Car2|Car3|Eno4|Fasn|Hadha|Thnsl2|Tor3a
GO:0016628	oxidoreductase activity, acting on the CH-CH group of donors, NAD or NADP as acceptor	MF	5	20	20	25	100	2,5701	0,0261	Dhcr24|Dhcr7|Fasn|Srd5a1|Tm7sf2
GO:0016491	oxidoreductase activity	MF	95	743	760	12,79	97,76	3,9571	0,0002	4833423E24Rik|Acad12|Acadl|Adhfe1|Adi1|Ado|Agmo|Akr1b8|Aldh18a1|Aldh1a2|Aldh1l1|Aldh1l2|Alkbh1|Alkbh8|Aoc2|BC026585|Cp|Cpox|Creg1|Cyb5r1|Cyb5r2|Cyb5r3|Cyba|Cybb|Cyp11a1|Cyp1b1|Cyp27a1|Cyp2a5|Cyp2j12|Cyp39a1|Cyp4a10|Cyp4f15|Cyp51|Dct|Dcxr|Ddo|Degs1|Dhcr24|Dhcr7|Dhfr|Dhrs1|Dio2|Ero1l|F8|Fa2h|Fads3|Fasn|Fdft1|Frrs1|Gpx8|Haao|Hadha|Hhip|Hmox1|Hpd|Hpgd|Hsd11b1|Hsd17b14|Idh1|Ifi30|Jmjd1c|Kdm2b|Kdm6b|Ldhd|Marc2|Me1|Mgst1|Moxd1|Mthfd2|Ncf1|Nsdhl|Phyhd1|Pipox|Plod1|Prdx4|Prodh|Pycr1|Qdpr|Rdh10|Rdh5|Rrm2|Sardh|Sc4mol|Sc5d|Sccpdh|Scd1|Scd2|Scd3|Sqle|Srd5a1|Tbxas1|Tet1|Tm7sf2|Vat1|Xdh
GO:2000377	regulation of reactive oxygen species metabolic process	BP	15	50	51	30	98,04	5,3186	0	Cdkn1a|Cryab|Foxm1|Gadd45a|Gstp1|Ier3|Il18|Nfe2l2|Tfap2a|Tgfb1|Thbs1|Trim30a|Trp53|Tspo|Xdh
GO:0000302	response to reactive oxygen species	BP	22	105	107	20,95	98,13	4,4302	0,0001	Anxa1|Apod|Atp7a|Bcl2|Cryab|Cyp11a1|Fabp1|Fos|Fosl1|Gstp1|Hmox1|Hyal1|Il18|Jun|Lcn2|Mdm2|Nfe2l2|Rela|Rhob|Star|Txnip|Ucp2

GO:0070482	response to oxygen levels	BP	35	223	225	15,7	99,11	3,683	0,0007	Adm|Agtrap|Ajuba|Apold1|Capn2|Casp1|Ccl2|Ccnb1|Cdkn1a|Cited2|Cryab|Cxcr4|Ddit4|Fabp1|Fas|Hmox1|Icam1|Il18|Lmna|Lpar1|Mdm2|Ndrg1|Pdlim1|Pdpn|Pgf|Plat|Plod1|Pml|Ryr1|S100b|Tgfb1|Tnfrsf1a|Trp53|Ucp2|Vcam1
GO:0050665	hydrogen peroxide biosynthetic process	BP	3	7	7	42,86	100	3,1914	0,0179	Cyba|Cybb|Ncf1
GO:0060263	regulation of respiratory burst	BP	3	8	8	37,5	100	2,8757	0,0269	Dusp10|Rac2|Rps19
GO:0045730	respiratory burst	BP	3	8	8	37,5	100	2,8757	0,0269	Cyba|Ncf1|Slc11a1
WP1496	oxidative damage	WP	13	42	44	30,95	95,45	3,6021	0,0014	Bcl2|C1qa|C1qb|C1qc|C1ra|C3ar1|C4b|C5ar1|Cdkn1a|Cdkn1b|Gadd45a|Pcna|Tnfrsf1b
MP:0005388	respiratory system phenotype	MP	157	1115	1127	14,08	98,94	2,0718	0,0416	Abca1|Abl1|Adamts2|Adm|Adora2a|Adora3|Aldh1a2|Alpl|Ascl1|Atf3|Atf5|Atp7a|Bag3|Bcl2|Bcl6|C3ar1|Casp8|Cd14|Cd44|Cd72|Cdkn1a|Cdkn1b|Cdon|Cebpg|Cited2|Clca1|Clec7a|Cmklr1|Cnp|Csf2rb|Ctsh|Ctsk|Ctss|Cxadr|Cxcr4|Cyba|Cysltr1|Cysltr2|Derl2|Dhcr7|Dock1|Dok7|E2f7|E2f8|Ednrb|Egfr|Egr2|Elk3|Erbb3|Fas|Fcgr2b|Fgfr2|Fgfr4|Flna|Flnc|Foxm1|Frem1|Fuz|Gja1|Gsn|Hbegf|Hck|Hey2|Hhip|Hip1|Hmox1|Hopx|Hsd11b1|Hspb11|Hspb8|Hyal1|Ift74|Igf2|Il12b|Il13ra1|Il17rb|Il1r1|Il2rg|Il33|Inpp5d|Insm1|Itga6|Itgb4|Jam3|Jun|Jup|Kdm6b|Klf3|Lcp2|Ldb3|Lgals3|Lhx2|Lilrb4|Lmna|Lpar4|Lrp2|Lrp4|Lyn|Mafb|Map3k14|Met|Myd88|Ncf1|Nckap1l|Nek6|Neurod1|Nfe2l2|Nfkb2|Ngfr|Notch2|Npc1|P2ry6|Pcsk6|Pdpn|Pla2g4a|Plat|Polr2a|Prkcq|Prrx1|Ptpn6|Rdh10|Rela|Relb|Runx1|Runx2|Rxfp1|Ryr1|S1pr3|Sc5d|Selp|Serpine1|Sesn2|Sh3gl3|Slc6a9|Sox2|Sox4|Sox9|Sp7|Spef2|Spry2|Sqle|Stat3|Stk40|Suv420h2|Tfap2a|Tgfb1|Tgfbr1|Thbs1|Timp1|Timp3|Tlr2|Tlr3|Tlr4|Tnfrsf1a|Tnfrsf1b|Tubb2b|Zfp36